EBioMedicine 69 (2021) 103456

Contents lists available at ScienceDirect

EBioMedicine

journal homepage: www.elsevier.com/locate/ebiom

Research paper

Loss of TRIM21 alleviates cardiotoxicity by suppressing ferroptosis induced by the chemotherapeutic agent doxorubicin

Kai Hou[a,b,c,d], Jianliang Shen[c], Junrong Yan[c], Chuannan Zhai[a,d], Jingxia Zhang[d], Ji-An Pan[e], Ye Zhang[f], Yaping Jiang[g], Yongbo Wang[b], Richard Z. Lin[g], Hongliang Cong[a,d,*], Shenglan Gao[b,*], Wei-Xing Zong[c,h,*]

[a] School of Medicine, Nankai University, Tianjin, China
[b] Department of Cellular and Genetic Medicine, School of Basic Medical Sciences, Fudan University, Shanghai, China
[c] Department of Chemical Biology, Ernest Mario School of Pharmacy, Rutgers University, Piscataway, NJ, USA
[d] Department of Cardiology, Tianjin Chest Hospital, Tianjin, China
[e] Department of Biochemistry and Molecular Cell Biology, School of Medicine, Sun Yat-sen University, Shenzhen, China
[f] Tianjin Third Central Hospital, Tianjin, China
[g] Department of Physiology and Biophysics, Stony Brook University, Stony Brook, NY, USA
[h] Rutgers Cancer Institute of New Jersey, New Brunswick, NJ, USA

ARTICLE INFO

Article History:
Received 13 January 2021
Revised 9 June 2021
Accepted 10 June 2021
Available online xxx

Keywords:
TRIM21
Antioxidant
Doxorubicin
Cardiotoxicity
Ferroptosis

ABSTRACT

Background: Doxorubicin, an anthracycline chemotherapeutic agent, is widely used in the treatment of many cancers. However, doxorubicin posts a great risk of adverse cardiovascular events, which are thought to be caused by oxidative stress. We recently reported that the ubiquitin E3 ligase TRIM21 interacts and ubiquitylates p62 and negatively regulates the p62-Keap1-Nrf2 antioxidant pathway. Therefore, we sought to determine the role TRIM21 in cardiotoxicity induced by oxidative damage.

Methods: Using TRIM21 knockout mice, we examined the effects of TRIM21 on cardiotoxicity induced by two oxidative damage models: the doxorubicin treatment model and the Left Anterior Descending (LAD) model. We also explored the underlying mechanism by RNA-sequencing of the heart tissues, and by treating the mouse embryonic fibroblasts (MEFs), immortalized rat cardiomyocyte line H9c2, and immortalized human cardiomyocyte line AC16 with doxorubicin.

Findings: TRIM21 knockout mice are protected from heart failure and fatality in both the doxorubicin and LAD models. Hearts of doxorubicin-treated wild-type mice exhibit deformed mitochondria and elevated level of lipid peroxidation reminiscent of ferroptosis, which is alleviated in TRIM21 knockout hearts. Mechanistically, TRIM21-deficient heart tissues and cultured MEFs and H9c2 cells display enhanced p62 sequestration of Keap1 and are protected from doxorubicin-induced ferroptosis. Reconstitution of wild-type but not the E3 ligase-dead and the p62 binding-deficient TRIM21 mutants impedes the protection from doxorubicin-induced cell death.

Interpretation: Our study demonstrates that TRIM21 ablation protects doxorubicin-induced cardiotoxicity and illustrates a new function of TRIM21 in ferroptosis, and suggests TRIM21 as a therapeutic target for reducing chemotherapy-related cardiotoxicity.

1. Introduction

Adverse cardiovascular events such as heart failure, myocardial infarction, and arrhythmias are major risks of anthracycline-based cancer chemotherapies [1]. Doxorubicin was discovered in the 1950s and has become one of the cornerstones of chemotherapy due to its high potency in a wide spectrum of solid and hematopoietic cancers. However, its clinical usage is severely limited due to cardiomyopathy and congestive heart failure [1-5]. Doxorubicin-induced cardiotoxicity may occur as early as after the first dose in patients [6-8]. Acute cardiac dysfunction also reflect myocyte injury that may eventually evolve into irreversible cardiotoxicity [6].

A main mechanism of doxorubicin-induced cardiotoxicity is thought to be increased oxidative stress [9-11]. A number of factors such as mitochondrial respiration, nitric oxide synthetases (NOSs), NAD(P)H oxidases, and catalase can be affected by doxorubicin

* Corresponding author.
E-mail addresses: hongliangcong@163.com (H. Cong), sgao@fudan.edu.cn (S. Gao), zongwx@rutgers.edu (W.-X. Zong).

https://doi.org/10.1016/j.ebiom.2021.103456

leading to oxidative stress and cardiomyocyte injury [12]. A major mechanism of increased oxidative stress involves the Kelch-like ECH-associated protein 1 (Keap1)-Nuclear factor E2-related factor 2 (Nrf2) antioxidant pathway [13,14]. Nrf2 is a member of the Cap-n-Collar family of basic leucine zipper proteins and it is regarded as a major anti-oxidative regulator through increasing the transcription of anti-oxidant genes [15-17]. Under basal conditions, Keap1 binds to Nrf2 and facilitates ubiquitination and degradation of Nrf2 in the cytoplasm by CUL3-containing E3 ubiquitin ligase. Under oxidative stress, Keap1 is dissociated from Nrf2 via the oxidation of its cysteine residues or via its sequestration by SQSTM1/p62, both leading to Nrf2 stabilization, nuclear translocation, and transcriptional activation of antioxidant response element (ARE)-containing genes [18-20]. Nrf2 transcriptional targets are involved in mediating iron metabolism, detoxification of reactive intermediates, and glutathione synthesis, all help alleviate oxidative stress.

Cardiac oxidative stress is known to cause cell death of cardiomyocytes and plays an important role in the pathogenesis of heart failure with reduced ejection fraction [1,4,21]. Several forms of cell death have been described during anthracycline-induced cardiotoxicity [22-26]. Ferroptosis, a form of cell death that is initiated by iron-dependent lipid peroxidation of the cell membrane, is associated with cellular antioxidant capacity and has been reported to be induced by doxorubicin, hence is a potential target for protection against doxorubicin-induced cardiotoxicity [24,27].

We recently reported that the ubiquitin E3 ligase TRIM21 (tripartite motif-containing protein 21) interacts and ubiquitylates p62, hence prevents p62 oligomerization and Keap1 sequestration and negatively regulates the p62-Keap1-Nrf2 antioxidant pathway. Loss of TRIM21 increases p62-Keap1-Nrf2 antioxidant capacity [28]. In the current study, we sought to study the effects of TRIM21 on doxorubicin-induced cardiotoxicity using mice with genetic ablation of TRIM21. We report here that TRIM21 knockout mice are protected from doxorubicin-induced heart failure and animal fatality. Mechanistically, this protection is attributed by increased p62-Keap1-Nrf2 antioxidant capacity and suppression of ferroptosis. Our study illustrates a new function of TRIM21 in ferroptosis and cardiotoxicity and suggests it as a potential therapeutic target for decreasing doxorubicin-induced cardiotoxicity.

2. Materials and methods

2.1. Mouse experiments

TRIM21 KO mice with C57BL/6J background were kind gift from Dr. Keiko Ozato. All mice experiments were done in compliance with the Institutional Animal Care and Use Committee guidelines at Rutgers University (PROTO201800127) and Stony Brook University (235160). Only male mice were used in this study due to a significant gender difference to doxorubicin induced cardiotoxicity. Hearts were isolated from the *TRIM21*$^{+/+}$ or *TRIM21*$^{-/-}$ C57BL/6J mice and then washed in the cold PBS. 10-20 mg tissues were lysed in 200-500 μl RIPA buffer with 1% SDS and homogenized. For fractionation assay, heart tissues were homogenized and separated into detergent (1% Triton X-100)-soluble "S" and insoluble "I" fractions. Samples were spun down at 12,000 x g for 10 min.

2.2. Doxorubicin treatment in vivo

For doxorubicin (MCE, NJ, USA, cat# HY-15142) treatment, 10-12 week-old male mice were weighted and then randomly received a single dose of doxorubicin (20 mg/kg) or equal volume of saline via intraperitoneal (i.p.) injection. For cardiac function examination, 5 days after doxorubicin treatment, mice were weighted, then cardiac functions of mice were measured by echocardiography. Mice were then sacrificed and hearts harvested for histology and immunohistochemistry analyses.

2.3. Left anterior descending (LAD) ligation

Mice were anesthetized with ketamine (80 mg/kg body weight) and xylazine (8 mg/kg). The neck area and the left side of rib cage were shaved and disinfected using 10 %(v/v) providone-iodine solution. A midline cervical incision was made to expose the trachea and the mouse was intubated below the glottis. Mice were ventilated using MiniVent (Model 845 Harvard Apparatus). Mice were then turned on the right side and a left thoracotomy was performed between the 2nd and 3rd intercostal space. Under microscopic view, the LAD was ligated on the proximal end located between the pulmonary artery and left auricle using a 6-O prolene suture (Ethicon). A 24-gauge chest tube was then placed to reinflate the lung after the thoracic incision is closed by sutures. The tracheal tube was removed and a single stitch suture was used to close the cervical incision with 5-O silk suture.

2.4. Echocardiography

Mice were anesthetized with isoflurane. Visual Sonics Vevo2100 Imaging System was used to measure heart rate and left ventricular dimensions from 2D short-axis under M-mode tracings at the level of the papillary muscle. Cardiac functional parameters, including ejection fraction, fractional shortening, and LVIDd (left ventricular internal diameter at end-diastole) were calculated by the Vevo software.

2.5. Histology and immunohistochemistry analyses

Heart tissues were fixed and processed for H&E and IHC staining for p62, ubiquitin, Nrf2, NQO1 and 4-HNE. In brief, hearts were fixed overnight in 4% paraformaldehyde (pH 7.4), embedded in paraffin, and sectioned at 5 μm thickness. Paraffin-embedded heart sections were deparaffinized, rehydrated, and microwave heated for 20 min in 0.01 mol/L citrate buffer (pH 6.0) for antigen retrieval. 3% hydrogen peroxide was applied to block endogenous peroxidase activity. After 30 min of blocking with goat serum, primary antibodies or control IgG were applied and incubated overnight at 4℃. After wash, slides were incubated with secondary antibody for 1 hour at room temperature with an interval washing. After rinsing with PBS, the slides were immersed for 5 min in the coloring substrate 3,3'-diaminobenzidine, counterstained with hematoxylin, dehydrated, and covered with coverslip.

2.6. Transmission electron microscopy

Myocardium (1 mm^3) was quickly removed from the left ventricle and immediately fixed in cold 2.5% phosphate-glutaraldehyde. Samples were embedded, cut, and mounted. Samples were observed using a Hitachi (80 kv) transmission electron microscope. Extent of mitochondrial damage was quantified using the Flameng score. For each sample, five fields were selected randomly, and 10 mitochondria were examined in each field.

2.7. Measurement of MDA content

Cells and cardiac malondialdehyde (MDA) levels were measured using a kit (Cat#S0131, Beyotime, Shanghai, China) in accordance with the manufacturer's instructions.

2.8. Cell cultures and in vitro treatment

Mouse embryonic fibroblasts (MEFs) was generated as previously described [28]. H9c2 immortalized rat cardiomyocyte line was

purchased from and authenticated by Shanghai Zhong Qiao Xin Zhou Biotechnology Co. (cat# ZQ0102, Shanghai, China). H9c2 cells were cultured in Dulbecco's modified Eagle's medium supplemented with 10% FBS (HyClone, UT, USA), 100 units/ml penicillin, and 100 μg/ml streptomycin. AC16 immortalized human cardiomyocyte line was purchased from and authenticated by Bluefbio Biotechnology Development Co. (cat# BFN60808678, Shanghai, China). AC16 cells were cultured in Dulbecco's modified Eagle's medium supplemented with 20% FBS (HyClone, UT, USA), 100 units/ml penicillin, and 100 μg/ml streptomycin. Mycoplasma testing has been performed and there was no mycoplasma contamination. Cells were incubated at 37°C in a humidified atmosphere containing 5% CO_2 and 95% air. Doxorubicin (MCE (MedChemExpress), NJ, USA, cat# HY-15142), Ferrostatin-1 (MCE, NJ, USA, cat# HY-100579), zVAD (MCE, NJ, USA, cat# HY-16658B), Necrostain-1 (MCE, NJ, USA, cat# HY-15760), ML385 (Cat# HY100523, MCE, NJ, USA) were applied at indicated concentrations.

2.9. Plasmids

Human TRIM21 construct and the TRIM21 LD and W381/383A mutants were described previously [28]

2.10. Transfection and infection for overexpression and knockdown

8×10^5 HEK293T cells were seeded in 6 cm dishes. After overnight recovery, for stable overexpression cell lines, cells were transfected with 0.5 μg VSVG, 1.5 μg helper, and 2 μg LPC vectors carrying HA-TRIM21 WT, HA-TRIM21 C16A, HA-TRIM21W381/383A by Lipofectamine 2000 (Invitrogen, CA, USA). For knockdown cell lines, HEK293T cells were transfected with 0.5 μg VSVG, 1.5 μg ΔR8.9, and 2 μg pLKO-shRNA constructs by Lipofectamine 2000. Human shNrf2 was cloned into pLKO-BSD and the rest shRNAs were cloned into pLKO-puromycin. Virus-containing medium was collected and mixed with complete DMEM medium at a ratio of 2:1. 5×10^5 target cells (MEFs, H9c2, and AC16) were plated in 6 cm dishes. The target cells were cultured with viral medium containing 0.1% polybrene, and selected by puromycin (2 μg/ml) for 3 days or by BSD (5 μg/ml) for 3 days.

The pLKO-shRNA against human TRIM21 was described previously [28]. The following oligos were used to generate shRNA targeting rat TRIM21, human Nrf2, and mouse Nrf2:

Rat shTRIM21-1:

Forward oligo:5'-CCGGGGTTCAGAACTGGAGCTATTGCTCGAGCAA T AGCTCCAG

TTCTAACCTTTTTG-3'

Reverse oligo:5′-AATTCAAAAAGGTTCAGAACTGGAGCTATTGCTCG AGCAATAGC

TCCAGTTCTAACC-3'

Rat shTRIM21-2

Forward oligo:

5'CCGGGCATTGTCTCCTTCTACAACACTCGAGTGTTGTAGAAGGAGA CAATGCTTTTTG3'

Reverse oligo: 5′AATTCAAAAAGCATTGTCTCCTTCTACAACACTCGA GTGTTGTAGAAGGAGACAATGC3'

Human shNRF2-1:

Forward oligo:

5′CCGGGGTTGAGACTACCATGGTTCCCTCGAGGGAACCATGGTAGT CT CAACCTTTTTG3′

Reverse oligo:

5′AATTCAAAAAGGTTGAGACTACCATGGTTCCCTCGAGGGAACCAT GGTAGTCTCAACC3′

Human shNRF2-2:

Forward oligo:

5′CCGGGCAGTTCAATGAAGCTCAACTCTCGAGAGTTGAGCTTCATT GAACTGCTTTTTG3′

Reverse oligo:

5′AATTCAAAAAGCAGTTCAATGAAGCTCAACTCTCGAGAGTTGAG CTTCATTGAACTGC3′

Mouse shNrf2-1

Forward oligo:

5′CCGGGCAGGACATGGATTTGATTGACTCGAGTCAATCAAATCCA TGTCCTGCTTTTTG3′

Reverse oligo:

5′AATTCAAAAAGCAGGACATGGATTTGATTGACTCGAGTCAATCAAA TCCATGTCCTGC3′

Mouse shNrf2-2

Forward oligo:

5′CCGGGGAGGCAGCCATGACTGATTTCTCGAGAAATCAGTCATGGC TGCCTCCTTTTTG3′

Reverse oligo:

5′AATTCAAAAAGGAGGCAGCCATGACTGATTTCTCGAGAAATCAGTCA TGGCTGCCTCC3′

2.11. Cell death assay

Cell death was quantified by Trypan Blue staining. 0.1 ml of cells (1×10^5 cells/ml) were mixed with 0.1 ml of 0.4% Trypan Blue and incubated at room temperature for 5 min. Cells were counted under a phase-contrast light microscope.

2.12. Western blot analyses

For total proteins, cells or tissues were lysed in RIPA buffer containing 1% SDS. After sonication on ice, samples were spun down at 12,000 x g for 10 min, and the supernatant was collected. For fractionation assay, cells or heart tissues were homogenized and separated into detergent (1% Triton X-100)-soluble "S" and insoluble "I" fractions. Protein concentration in the supernatant was measured using the BCA Protein Assay Kit (cat# P0012, Beyotime, Shanghai, China). A total of 10-30 μg protein per sample was resolved in a 7.5-12.5% SDS-PAGE and transferred to a nitrocellulose membrane. The membranes were blocked with 5% BSA in PBS containing 0.05% Tween-20, then incubated with primary antibodies at 4°C overnight.

2.13. RNA-sequencing and data analysis

Total RNA was isolated from heart tissues using a Kit (PureLink™ RNA Mini Kit, Cat#12183018A, Invitrogen, USA). RNA purity was determined by NanoPhotometer® (IMPLEN, CA, USA). RNA concentration and integrity were measured with Agilent 2100 Bioanalyzer using Agilent RNA 6000 Nano Kit (Agilent Technologies, CA, USA). Approximately 1 μg total RNA was used for RNA-seq library preparation with VAHTS Universal V6 RNA-seq Library Prep Kit for Illumina (#NR604, Vazyme Biotech, Nanjing, China) according to manufacturer's instructions. Briefly, the poly-A containing mRNA was firstly purified with poly-T oligo-attached magnetic beads. mRNA was then fragmented into small pieces using Fragmentation buffer and synthesized to first strand cDNA with reverse transcriptase and random primers. Later, the second strand cDNA was synthesized with dNTPs, RNase H and DNA Polymerase I. After purification, double strand cDNAs were subjected to end repair process, addition of a single 'A' base, and ligation of sequencing adapters. The products were then purified and enriched with PCR to create the final RNA-seq library. The RNA-seq libraries were then subjected to quality control, pooled for cBot amplification and 150 bp paired-end reads sequencing run with Illumina NovaSeq 6000 platform. An average of 20 M reads were obtained for the set of samples.

The raw reads were aligned to the Mus_musculus genome reference (UCSC mm10) using Bowtie2,[29] and genes were annotated and quantified by featureCounts[30]. DEseq was used to identify

differentially expressed genes (DEGs) [31]. Genes with sequencing read counts ≥1 in at least one comparison condition were used for the analysis. DEGs induced by doxorubicin treatment in Trim21 knock-out samples were identified by Fold Change (FC) ≥ 2 and Benjamini & Hochberg (BH)-adjusted *p* value ≤ 0.1, and those in Trim21 wild-typeknock-out samples were identified by Fold Change (FC) ≥ 2 among the top 500 genes in k-means cluster. Gene ontology (GO) analysis was performed using metascape (https://metascape.org/) [32]. Plots were generated and the related statistics were conducted using R version 3.6.1.

To analysis TRIM21 in human heart failure and in doxorubicin-treated mouse heart injury in publicly available datasets, GEO datasets were downloaded.

2.14. Quantitative real-time PCR

Total RNA was isolated from heart tissues using a Kit (PureLink™ RNA Mini Kit, Cat#12183018A), and RNA concentration and purity were measured using a spectrophotometry. RNA was reverse-transcribed using the HiScript II Q RT SuperMix for qPCR Kit (Cat# R223-01, Vazyme, Nanjing, China) in accordance with the manufacturer's instructions. Quantitative PCR was performed using a QuantStudio 3 (ABI) and Hieff qPCR SYBR Green Master Mix (Cat#11203ES08, YEASEN, Shanghai, China) in accordance with the manufacturer's instructions. The fold difference in gene expression was calculated using the $2^{-\triangle\triangle Ct}$ method and is presented relative to *GAPDH* mRNA. All reactions were performed in triplicate, and specificity was monitored using melting curve analysis. Following PCR primers were used: mouse *TRIM21*, 5'-GGGAGGAGGTCACCTGTTCTA-3' and 5'-GGCACTCGGGACATGAACTG-3'; mouse *NQO1*, 5'-AGGATGGGAGGTACTCGAATC-3' and 5'-AGGCGTCCTTCCTTATATGCTA-3'; mouse *NRF2*, 5'-CTGAACTCCTGGACGGGACTA-3' and 5'-CGGTGGGTCTCCGTAAATGG-3'; mouse *PTGS2*, 5'-CTGCGCCTTTTCAAGGATGG-3' and 5'-GGGGATACACCTCTCCACCA-3'; mouse *BNP*, 5'-AAGTCCTAGCCAGTCTCCAGA-3' and 5'-GAGCTGTCTCTGGGCCATTTC-3'; mouse *MYH7*, 5'-GCTGAAAGCAGAAAGAGATTATC-3' and 5'-TGGAGTTCTTCTCTTCTGGAG-3'; mouse *GAPDH*, 5'-ATCATCCCTGCATCCACT-3' and 5'-ATCCACGACGGACACATT-3'; mouse *Hmox1*, 5'-GGTGATGGCTTCCTTGTACC-3' and 5'-AGTGAGGCCCATACCAGAAG-3'; mouse *SLC7A11*, 5'-GGCACCGTCATCGGATCAG-3' and 5'-CTCCACAGGCAGACCAGAAAA-3'; human *SLC7A11*, 5'-TCTCCAAAGGAGGTTACCTGC-3' and 5'-AGACTCCCCTCAGTAAAGTGAC-3'; mouse *GPX4*, 5'-GCCTGGATAAGTACAGGGGTT-3' and 5'-CATGCAGATCGACTAGCTGAG-3'; mouse *FTH*, 5'-CCATCAACCGCCAGATCAAC-3' and 5'-GAAACATCATCTCGGTCAAA-3'; mouse *FTL*, 5'-CGTCTCCTCGAGTTTCAGAAC-3' and 5'-CTCCTGGGTTTTACCCCATTC-3'; human *GAPDH*, 5'-ACAACTTTGGTATCGTGGAAGG-3' and 5'-GCCATCACGCCACAGTTTC-3'; mouse GSTM1, 5'-TTTGTCCTGCCCACGTTTCT-3' and 5'-TCAAAGTCGGGAGCGTCAC-3'; mouse GSTM2, 5'-TGGACTTTCCCAATCTGCCC-3' and 5'-ATCTTCTCAGGGAGACCCTCT-3'; mouse GSTM4, 5'-AGCTCACGCTATTCGGCTG-3' and 5'-GCTCCAAGTATTCCACCTTCAGT-3'; mouse GSTM5, 5'-TCATCCAAGTCTATGGTTCTGGG-3' and 5'-CCACAGATGTACCGTTTCTCCT-3'; mouse GSTM7, 5'-GATGAGGCTTTACTCTGAGTTCC-3' and 5'-AGCAATGAAATCCACAAAGGTGA-3'; mouse GPX2, 5'-TCGGACATCAGGAGAACTGTC-3' and 5'-CGCACGGGACTCCATATGAT-3'

2.15. Antibodies

Anti-p62 (Novus, cat#H00008878-M01, RRID: AB_437085, 1:200 for IHC, 1:4,000 for WB), anti-ubiquitin (Abcam, cat#ab7780, RRID: AB_306069, 1:200 for IHC), anti-Nrf2 (Abcam, cat#ab62352, RRID: AB_944418, 1:200 for IHC, 1:1,000 for WB), anti-NQO1(ABclonal, cat#A19586, RRID: AB_2862684, 1:200 for IHC, 1:1,000 for WB), anti-4-HNE (Abcam, cat#ab46545, RRID: AB_722490, 1:200 for IHC), caspase 3 (Proteintech, cat#19677-1-AP, RRID: AB_10733244, 1:1,000 for WB), tubulin (Proteintech, cat#11224-1-AP, RRID: AB_2210206, 1:2,000 for WB), Keap1 (Proteintech, cat#10503-2-AP, RRID: AB_2132625, 1:1,000 for WB). All the antibodies above are commercial antibodies. They are authenticated by companies. Relevant documentations were provided in Supplemental Data.

2.16. Statistical analysis

Data were analyzed and graphed using GraphPad Prism software, and all summary data are presented as mean ± SD. For analysis between two groups, Student t-test is applied. One-way ANOVA with Tukey's post hoc test was used for comparisons between more than two groups. For the Kaplan-Meier survival plots, statistical significance was measured using the log-rank (Mantel-Cox) test. Correlation studies were done using Pearson Correlation Test**.** Results were considered significant when $p<0.05$.

2.17. Ethics statement

All the animal experiments were performed in compliance with the NIH Guide for the Care and Use of Laboratory Animals (National Academies Press, 2011) and were approved by the Animal Ethics committees of Rutgers University and Stony Brook University.

2.18. Role of funding source

Funders provide financial support for this study, and do not participate in study design, data collection, data analyses, interpretation, or writing of report.

3. Results

3.1. Loss of TRIM21 has cardio-protective effects in two mouse models of cardiac injury

Various treatment regimens have been reported to study doxorubicin cardiotoxicity in mouse models, including using very low-dose doxorubicin to avoid systemic toxicity [33]. We used an acute cardiotoxicity model that was induced by single injection of doxorubicin [24,34-37]. *TRIM21*$^{+/+}$ and *TRIM21*$^{-/-}$ C57BL/6J male mice (10-12 week) were randomly divided into two groups: one was injected intraperitoneally (i.p.) with 20 mg/kg of doxorubicin, and the other with same volume of saline. TRIM21 knockout (KO) mice do not show overt developmental defects,[28,38]. After doxorubicin treatment, TRIM21 KO mice survived significantly longer than the WT mice (Fig. 1a). WT but not KO mice showed an obvious hair loss, an adverse effect that has been described to associate with doxorubicin treatment (Fig. 1b) [39-41]. Meanwhile, we used another cohort of mice to monitor cardiac functions by transthoracic echocardiography. At the fifth day after doxorubicin injection, cardiac function was evaluated by transthoracic echocardiography. Doxorubicin treatment led to reduced ventricular wall motion (Fig. 1c), lower left ventricular ejection fraction (LVEF), fractional shortening (FS), heart-beat rate, and increased left ventricular internal diameter at end-diastole (LVIDd) in WT mice, and the symptoms were significantly alleviated in KO mice (Fig. 1d). These data suggest that the cardiac function in TRIM21 KO mice is better protected than that in WT mice. Doxorubicin treatment is a major cause of dilated cardiomyopathy and congestive heart failure[42], which is associated with splanchnic circulation congestion, leading to bowel wall edema and ascites [43]. Autopsy revealed that doxorubicin-treated WT displayed obvious ascites and enlarged hearts, signs of congestive heart failure (Fig. 1e and 1f). KO mice showed markedly smaller ascites volume and heart enlargement (Fig. 1e and 1f). Moreover, KO mice were better protected from doxorubicin-induced body weight loss which is a symptom of

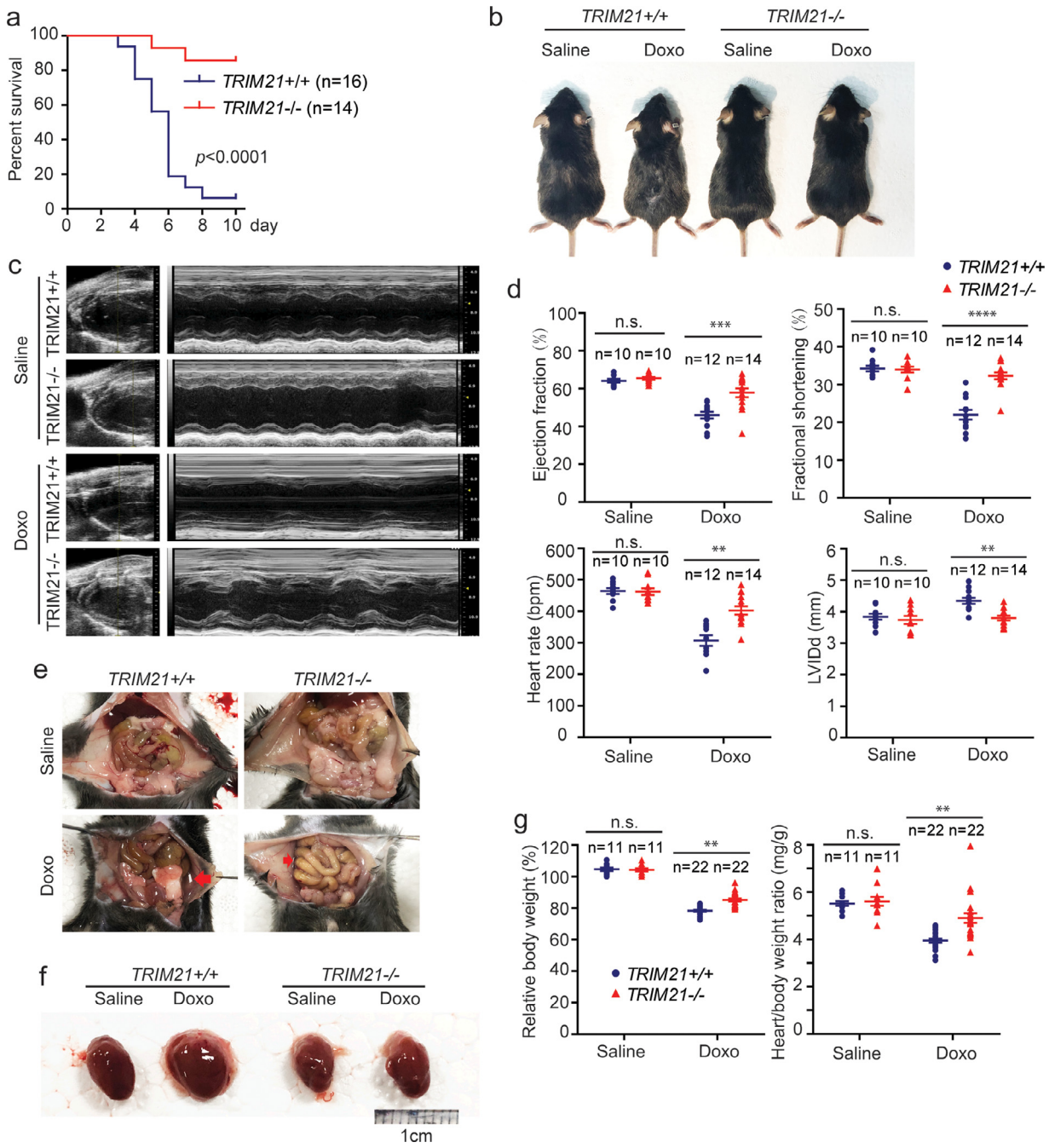

Fig. 1. Loss of TRIM21 has a protective effect on doxorubicin-induced cardiotoxicity in mice. *TRIM21*$^{+/+}$ or *TRIM21*$^{-/-}$ male mice (10 to 12 week-old) were treated with doxorubicin (20 mg/kg, i.p.). (a) Kaplan–Meier survival curves were generated. Log rank test was used to compare the difference in survival between *TRIM21+/+* (n=16) and *TRIM21-/-* (n=14), showing significant difference with p-value < 0.0001. (b) Mice were injected with saline or doxorubicin (20 mg/kg, i.p.). 5 days later, mice were photographed. Representative pictures are shown. Note doxorubicin-treated WT mice displayed smaller body weight and hair loss. (c) 5 days after doxorubicin injection, mice were subjected to echocardiography. (d) M-mode images from nine cardiac cycles for each animal were used to calculate ventricular measurements: ejection fraction, fractional shortening, heart rate, and LVIDd (left ventricular internal diameter at end-diastole). Individual data points and the mean ± standard deviation are shown. Student's t-test was used to compare the results. n.s., non-significant; **p<0.01; ***p<0.001; ****p<0.0001. (e) Abdominal photographs of mice after 5-days after doxorubicin injection. Abdominal ascites are indicated by red arrows. (f) Hearts from each group were photographed. Representative photos are shown. (g) Mice were weighted at the time of doxorubicin injection and 5 days after, relative body weight (normalized to body weight at the injection) and the heart/body weight ratio was measured. Each individual data point represents a mouse. Individual data points and the mean ± standard deviation are shown. Student's t-test was used to compare the results. n.s., non-significant; **p<0.01.

anorexia caused by heart failure associated bowel congestion, and the heart/body weight ratio of KO mice was also better preserved, consistent with reduced loss of cardiomyocyte (Fig. 1g).

As our TRIM21 knockout mouse is a global gene knockout strain, we examined the effect of TRIM21 ablation in a more cardiac-specific injury model that involves oxidative damage. The Left Anterior Descending (LAD) coronary artery was ligated in TRIM21 WT and knockout mice to cause myocardial infarction. The cardiac function of these mice was monitored longitudinally with echocardiography. Even at one week after LAD ligation there was a significant difference in ejection fraction between the two groups. The cardiac function of *TRIM21*$^{-/-}$ mice was significantly better at 1, 4 and 8 weeks after the procedure (Suppl. Fig. S1a and S1b). Left ventricular dilation caused by LAD ligation was also significantly alleviated by the loss of TRIM21

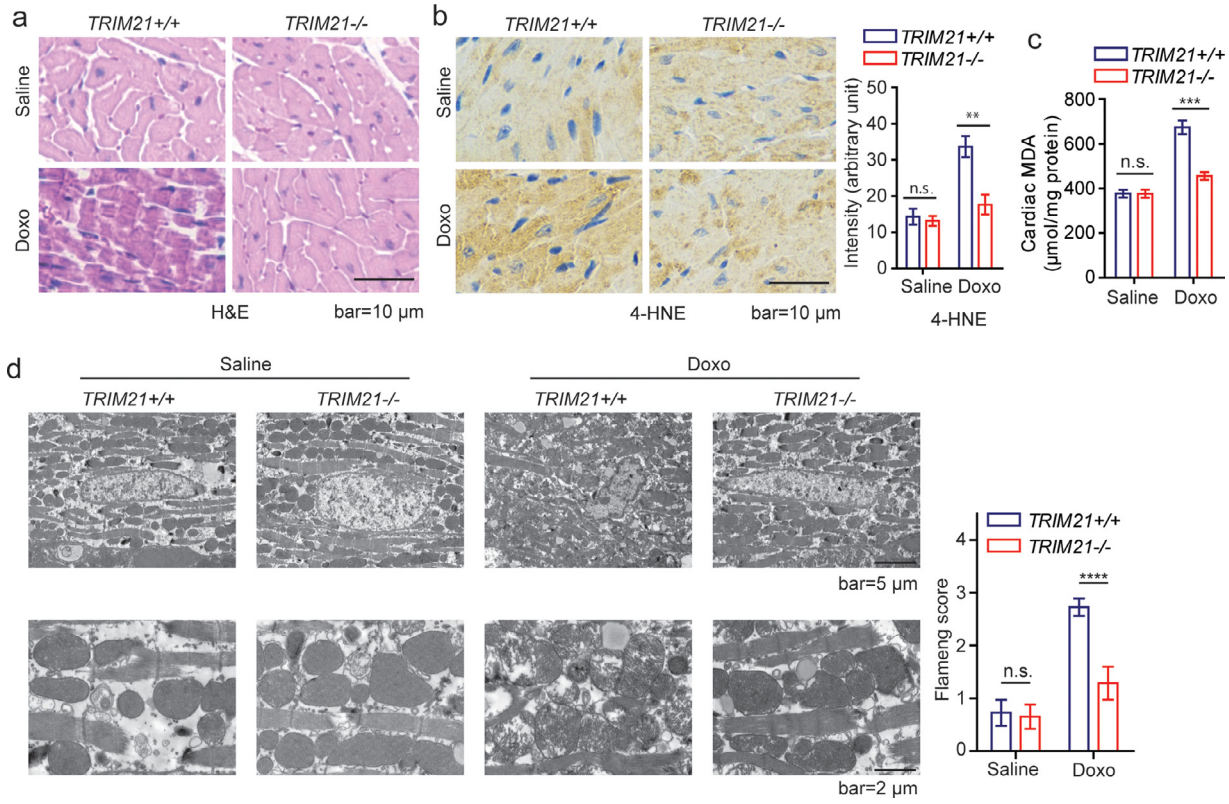

Fig. 2. TRIM21 ablation alleviates doxorubicin-induced cardiotoxicity. *TRIM21*$^{+/+}$ or *TRIM21*$^{-/-}$ mice (n=5 in each group) were injected with saline or doxorubicin (20 mg/kg via i.p.). 5 days later, hearts were isolated. (a) Representative H&E staining images are shown. (b) Hearts were collected and examined with 4-HNE IHC staining. The intensity was quantified by Image J. Data shown are mean ± standard deviation. Student's t-test was used to compare the results. n.s., non-significant; **p<0.01. (c) The level of MDA in the heart tissue was determined and the mean ± SD of triplicate experiments is shown. Student's t-test was used to compare the results. n.s., non-significant; ***p<0.001. (d) Transmission electron microscopy of heart tissues. Note deformed/damaged mitochondria in doxorubicin-treated *TRIM21*$^{+/+}$ hearts. The extent of mitochondrial damage was quantified using the Flameng score. Data shown are mean ± standard deviation. Student's t-test was used to compare the results. n.s., non-significant; ****p<0.0001.

(Suppl. Fig. S1c). Of note, cardiac contractility of the *TRIM21*$^{-/-}$ mice improved at 8 weeks as compared to 4 weeks. This is probably due to preservation of more viable cardiac myocytes surrounding the infarcted zone in the knockout group. As these myocytes recovered from the initial ischemic insult, cardiac contractility continue to improve. Since the ejection fraction *TRIM21*$^{-/-}$ mice at 8 weeks have recovered to the normal range, there is likely compensatory hypertrophic response by remaining myocytes in the heart. In contrast, cardiac contractility of WT mice did not recover with time suggesting a more lasting ischemic insult in the presence of TRIM21. In summary, these results indicate that loss of TRIM21 confers protection against heart-specific oxidative injury, consistent with our above results in the doxorubicin experiment.

3.2. *TRIM21-deficient hearts are protected from doxorubicin-induced ferroptosis*

Our above results indicate that loss of TRIM21 has a protective effect on two cardiac injury models: doxorubicin-induced cardiotoxicity and the LAD ligation-induced myocardial infarction in mice. Both models have been reported to involve dysregulated redox balance [21,44]. We then further explored the effect of TRIM21 on doxorubicin-induced cardiotoxicity. It has been suggested that doxorubicin-induced cardiomyopathy is mainly attributed to ferroptosis,[24] which is initiated by the perturbation of the intracellular microenvironment via ROS generation and iron-dependent lipid peroxidation [27]. Close examination of the heart tissues from doxorubicin-treated mice revealed disarrangement of cardiomyocytes and disappearance of myocardial stria in the WT but not TRIM21 KO mice (Fig. 2a). Lipid peroxidation markers 4-hydroxynonenal (4-HNE) and malondialdehyde (MDA) were markedly higher in the heart of WT but not KO mice after doxorubicin treatment (Fig. 2b and 2c). Transmission electron microscopy (TEM) revealed typical ferroptosis-associated mitochondrial abnormalities including disrupted cristae and compromised membrane integrity as previously reported,[45] which was drastically milder in the KO than WT mice (Fig. 2d). These results indicate that doxorubicin treatment induces ferroptosis in cardiomyocytes as previously reported(24), which can be suppressed upon TRIM21 ablation.

We further determined whether TRIM21 deficiency protects against cardiotoxicity by activating the p62-Keap1-Nrf2 antioxidant pathway. Western blotting (WB) (Fig. 3a) and immunohistochemistry (IHC) analyses (Fig. 3b) revealed that both Nrf2 and NQO1, which are transcription targets of Nrf2, were induced by doxorubicin treatment more significantly in the *TRIM21*$^{-/-}$ hearts. Consistent with our previous report that TRIM21 ablation leads to increased p62 sequestration of polyubiquitinated proteins,[28] doxorubicin also induced more aggregation of p62 and polyubiquitinated proteins (Fig. 3b) and sequestration of p62 and Keap1 in the detergent (1% Triton X-100) insoluble fractions (Fig. 3c). These results indicate that TRIM21 ablation leads to enhanced p62 sequestration of Keap1 and antioxidant capacity and subsequent protection against doxorubicin-induced ferroptosis in the heart.

3.3. *TRIM21 is associated with redox regulation*

To study the physiological relevance of TRIM21, we examined the expression of TRIM21 in human and mouse heart tissue samples using publicly available datasets. In human, no data with heart tissues in doxorubicin-induced heart failure patients could be found. In other

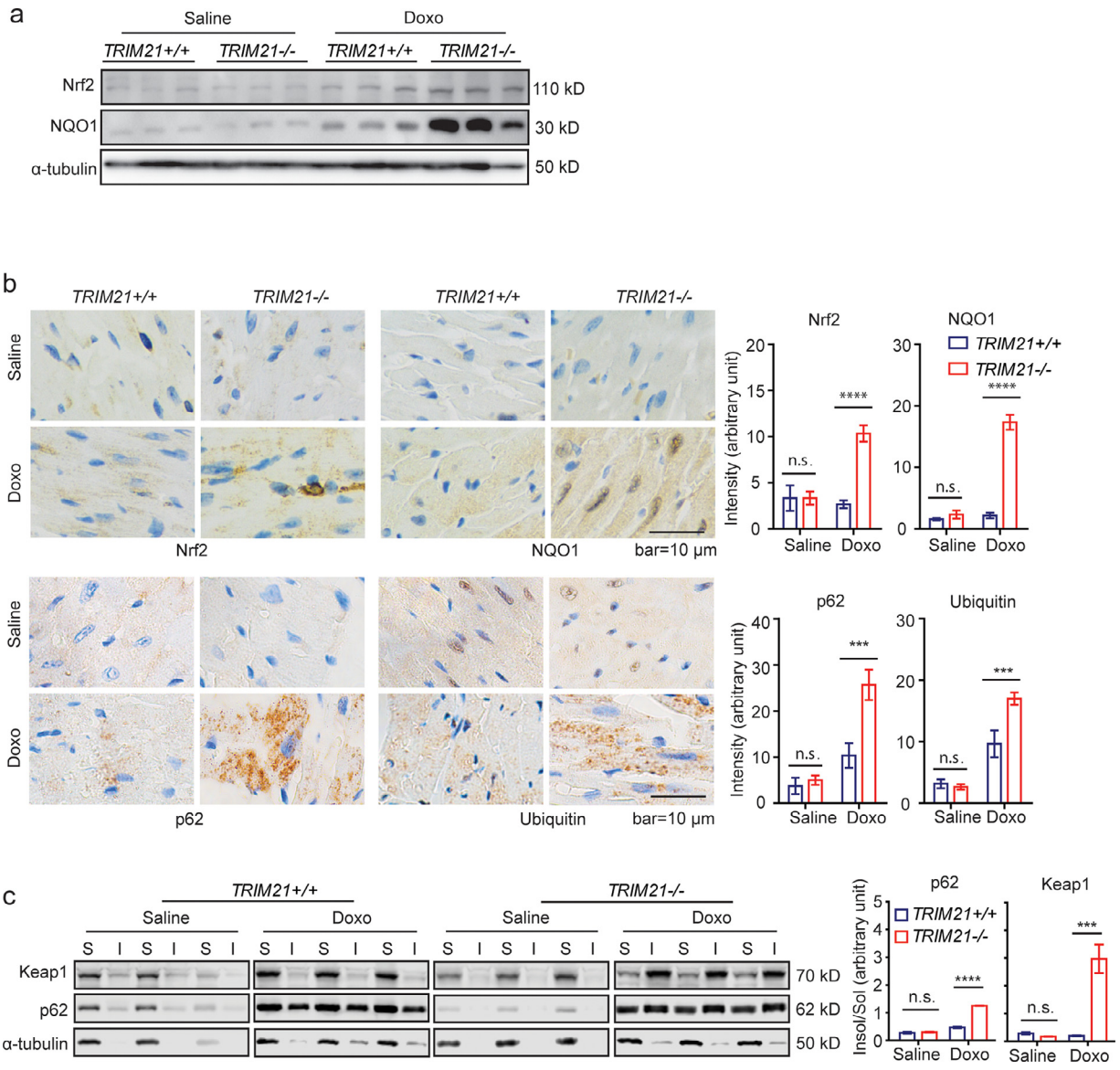

Fig. 3. TRIM21 negatively regulates p62-Keap1 aggregation and anti-ferroptotic effect in heart tissue. *TRIM21*$^{+/+}$ or *TRIM21*$^{-/-}$ mice (n=5 in each group) were i.p. injected with saline or doxorubicin (20 mg/kg). Heart tissues were harvested 5 days later. (a) Heart tissues were lysed in RIPA buffer containing 1% SDS and probed for indicated proteins. (b) IHC staining was performed for indicated antibodies. IHC intensity was determined and quantified by Image J. Data shown are mean ± standard deviation. Student's t-test was used to compare the results. n.s., non-significant; ***p<0.001, ****p<0.0001. (c) Heart tissues were lysed and separated into detergent (1% Triton X-100)-soluble "S" and insoluble "I" fractions and subjected to IB. The ratio of insoluble/soluble fractions was normalized to the corresponding tubulin band and is shown on the bottom. Densitometry of immunoblot bands was determined by the Odyssey Infrared Imaging System. Data shown are mean ± standard deviation. Student's t-test was used to compare the results. n.s., non-significant; ***p<0.001, ****p<0.0001.

redox-related heart conditions such as ischemic heart failure, 1 out of 5 studies detected increased TRIM21 expression in the ischemic heart failure samples (Fig. 4a). Interestingly, TRIM21 expression reversely correlates with GSTM4 and GPX4, two antioxidant molecules, and positively with PTGS2, a ferroptosis marker (Fig. 4b). In mice, one study (GSE40289) showed that TRIM21 was increased upon 16-hour doxorubicin treatment, while others showed no significant changes in TRIM21 expression upon doxorubicin treatment (Fig. 4c).

To further determine the effect of TRIM21 ablation on the heart tissue response to doxorubicin treatment, we performed RNA sequencing (RNA-seq) analysis of heart tissues of *TRIM21* WT or KO mice treated with doxorubicin then harvested 5 days later. Differentially expressed genes were identified by a cutoff of 2-fold and $p<0.05$ (Fig. 4d). Upon doxorubicin treatment, 500 genes were altered in *TRIM21* WT, 344 in *TRIM21* KO, with 175 genes in common (Fig. 4e). Gene ontology (GO) analysis revealed that the redox regulation and ion homeostasis pathways were among the remarkably altered in *TRIM21* WT or KO mice (Fig. 4f). Real-time quantitative reverse transcription PCR (qRT-PCR) analysis confirmed that doxorubicin did not cause drastic change of TRIM21 expression, consistent with most previous studies (Fig. 4c). Importantly, both Nrf2 and NQO1 were induced by doxorubicin treatment more significantly in the *TRIM21*$^{-/-}$ hearts (Fig. 4g), consistent with the results obtained by WB and IHC (Fig. 3a and 3b). Similarly, the expression levels of cardiomyopathy biomarkers brain natriuretic peptide (BNP) and slow skeletal/β-cardiac myosin heavy chain (MYH7) were markedly induced in the WT but not KO hearts. Interestingly, the putative ferroptosis markers prostaglandin-endoperoxide synthase 2 (PTGS2) and hemo oxygenase 1 (HMOX1) were also significantly up-regulated in the WT but with lower level in KO hearts (Fig. 4g), consistent with the human heart tissue analysis (Fig. 4b) and with the ferroptotic features observed by EM (Fig. 2d). It is interesting to note that cystine/glutamate antiporter (SLC7A11) was expressed at a much lower level in mouse hearts, and glutathione peroxidase 4 (GPX4) was not

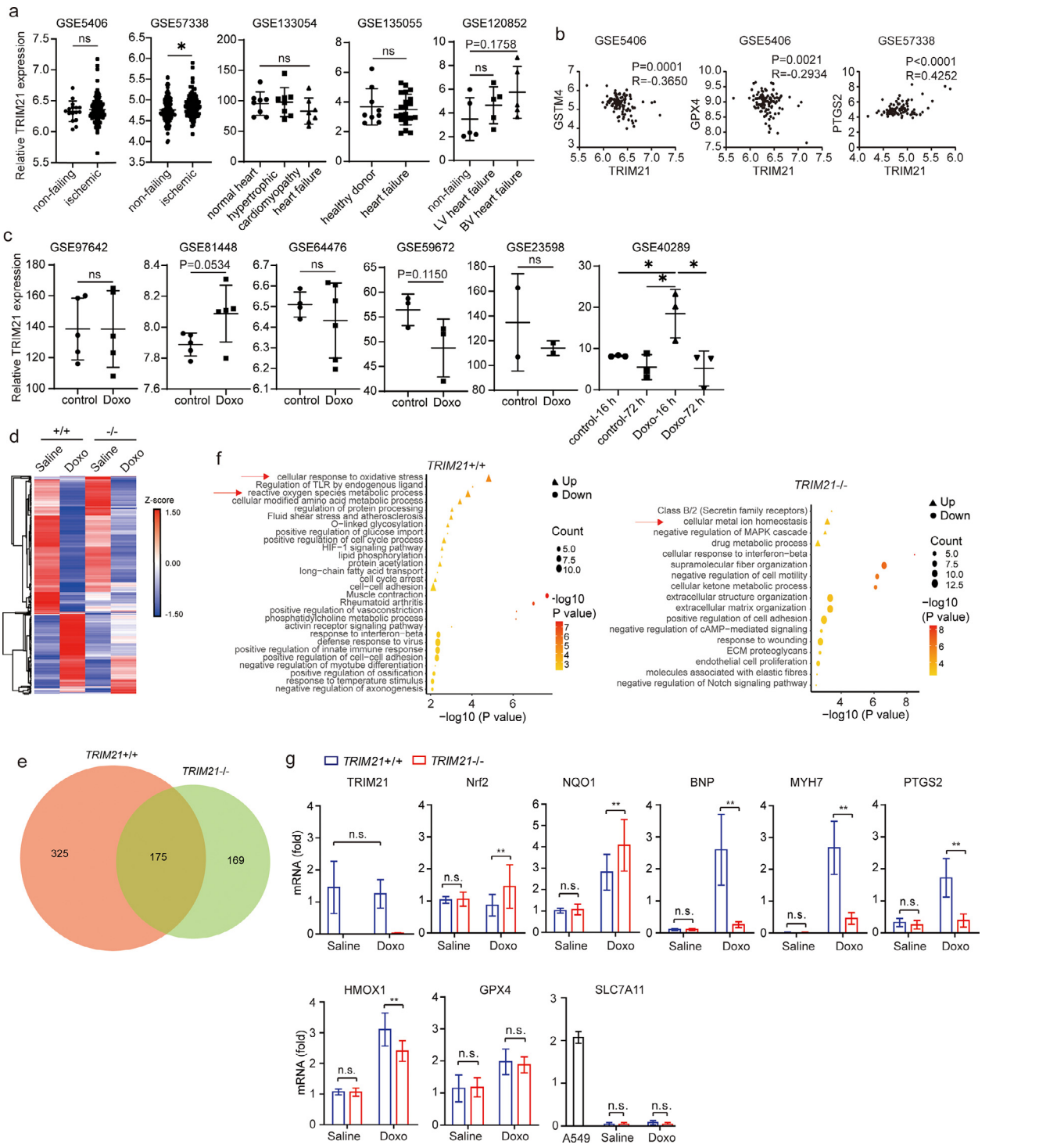

Fig. 4. Doxorubicin-induced cardiomyopathy and ferroptosis are suppressed in *TRIM21*$^{-/-}$ hearts. (a) Relative TRIM21 expression in human heart tissue samples under indicated conditions. TRIM21 expression levels were estimated by normalized probe intensity obtained from previously published microarray datasets, with Gene Expression Omnibus (GEO) accession number shown in each sub-figure. P values less than 0.2 are annotated. (b) Correlation between TRIM21 and indicated genes in indicated datasets. (c) Relative TRIM21 expression in mouse heart tissue samples upon doxorubicin (Doxo) treatment. TRIM21 expression levels were estimated by normalized probe intensity obtained from previously published microarray datasets, with Gene Expression Omnibus (GEO) accession number shown. P values less than 0.2 are annotated. (d) Ten to twelve week-old *TRIM21*$^{+/+}$ and *TRIM21*$^{-/-}$ male mice were treated with PBS or 20 mg/kg Doxo by intraperitoneal injection. Heart tissues were collected after 5 days and used for RNA-seq. Hierarchical clustering and heatmap illustration of differentially expressed genes under indicated conditions. Color key donates Z-scores after normalization. (e) Venn diagram showing overlap of genes differentially expressed in Doxo versus PBS-treated *TRIM21*$^{+/+}$ and *TRIM21*$^{-/-}$ mice. Analysis was restricted to genes with a 2-fold difference. (f) Dot plots showing the enriched terms from Gene Ontology analysis using differentially expressed genes identified from Doxo versus PBS treatment in TRIM21 wild-type and knockout mice. Note that pathways involved in redox regulation and metal ion homeostasis are identified. (g) Total mRNA was extracted and analyzed by qRT-PCR (n=5 in each group). Relative mRNA levels of indicated genes are shown as mean ± standard deviation. Note that A549 human lung carcinoma cell line was used as a control to demonstrate that SLC7A11 is expressed at a very low level in mouse heart tissues. Student's t-test was used to compare the results. n.s., non-significant; **p<0.01.

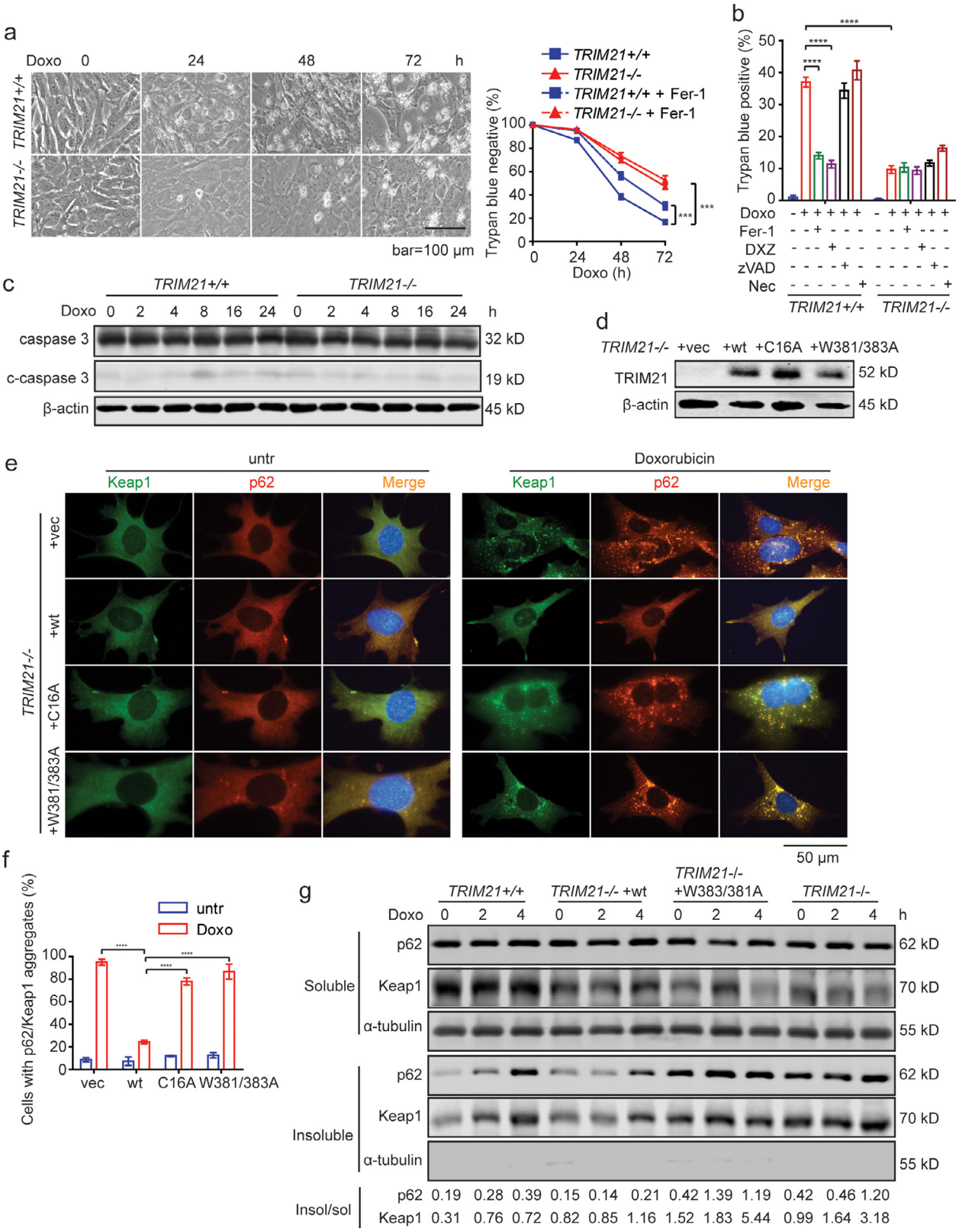

Fig. 5. TRIM21-deficient MEFs are protected from doxorubicin-induced ferroptosis. (a) *TRIM21*$^{+/+}$ or *TRIM21*$^{-/-}$ MEFs were treated with doxorubicin (0.1 μM) alone or together with ferrostatin-1 (Fer-1, 2 μM) for the indicated times. Cells were observed under phase-contrast microscope, and cell death determined by trypan blue staining. Data shown are the mean plus SD of three random countings (500 cells each). Student's t-test was used to compare the results at indicated times. ***p<0.001. (b) Cells were treated with doxorubicin (0.1 μM) in the presence of ferrostatin-1 (Fer-1, 2 μM), dexrazoxane (DXZ, 100 μM), zVAD (10 μM), or necrostatin-1 (Nec, 0.5 μM) for 36 h. Cell death was determined by trypan blue staining. Data shown are mean ± standard deviation. Student's t-test was used to compare the results. n.s., non-significant; ****p<0.0001. (c) Cells treated with doxorubicin (1 μM) for indicated times, and probed for caspase-3. (d) *TRIM21*$^{-/-}$ MEFs were reconstituted with vector, HA-TRIM21WT, HA-TRIM21C16A or HA-TRIM21W381/383A mutants. (e)*TRIM21*$^{-/-}$ MEFs reconstituted with WT TRIM21 or the mutants were treated with doxorubicin (1 μM) for 16 h. Immunofluorescence of indicated proteins was performed. Note that doxorubicin treatment induced Keap1 and p62 aggregation in *TRIM21*$^{-/-}$ MEFs, which was abrogated by the reconstitution of TRIM21 WT but not the ligase-dead C16A mutant or the p62 binding-deficient W381/383A mutant. (f) Quantification of (e). Data shown are mean ± standard deviation. Student's t-test

significantly altered in the *TRIM21* KO mice comparing with the WT mice (Fig. 4g).

3.4. TRIM21 negatively regulates p62-Keap1 aggregation and anti-ferroptotic effect in MEFs and cardiomyocytes

To test the effect of TRIM21 on ferroptosis induced by doxorubicin, we treated immortalized mouse embryonic fibroblasts (MEFs) isolated from TRIM21 WT and KO embryos [28]. Similar to the heart tissues (Fig. 5g), acute doxorubicin treatment induced significantly elevated expression of NQO1, NRF2, and several other NRF2 target genes such as GPX2, GSTM1, GSTM2, and GSTM4, whereas the expression of HMOX1 was lower in TRIM21-KO MEFs and that of SLC7A11 did not have significant change (Suppl. Fig. S2). Doxorubicin caused more profound cell death in WT MEFs, which could be rescued by the ferroptosis inhibitor ferrostatin-1 and the iron chelator dexrazoxane (Fig. 5a and 5b), but not by the apoptosis inhibitor zVAD or necroptosis inhibitor necrostatin-1 (Fig. 5b). Cleaved-caspase 3, which is indicative of apoptotic activation of caspase cascade, was not apparent upon doxorubicin treatment (Fig. 5c). We recently reported that the ubiquitin E3 ligase TRIM21 interacts with and ubiquitylates p62, hence prevents p62 oligomerization and Keap1 sequestration and negatively regulates the p62-Keap1-Nrf2 antioxidant pathway [28]. The E3 ligase-defective C16A mutant and the p62 interaction-defective W381/383A mutant cannot suppress p62 sequestration function and antioxidant capacity [28]. *TRIM21*$^{-/-}$ MEFs were reconstituted with WT TRIM21, the ligase-dead C16A, or the p62 binding-defective W381/383A mutants (Fig. 5d). Indeed, doxorubicin treatment induced p62 and Keap1 in *TRIM21*$^{-/-}$ MEFs, which was largely suppressed by the reconstitution of WT TRIM21, but not by the C16A or W381/383A mutants (Fig. 5e and 5f). Moreover, Triton X-100 fractionation revealed that reconstitution of WT TRIM21 but not the W381/383A mutants reduced the amount of Triton X-100 (1%)-insoluble fraction of p62 and Keap1 (Fig. 5g).

We then determined the effect of TRIM21 on doxorubicin induced cytotoxicity in an immortalized rat cardiomyocyte line H9c2, which is widely used in cardiology studies [24,46,47]. TRIM21 was stably silenced by two independent lentiviral short-hairpin RNAs (shRNAs) of TRIM21 in H9c2 cells. Successful silencing was verified by quantitative reverse-transcript PCR (qRT-PCR) (Fig. 6a) due to the lack of antibodies that recognize rat TRIM21. Silence of TRIM21 led to protection against doxorubicin-induced cell death (Fig. 6b). Similar as in MEFs (Fig. 5b), doxorubicin-induced cell death was inhibited by the ferroptosis inhibitor ferrostatin-1 and the iron chelator dexrazoxane but not the apoptosis inhibitor zVAD or necroptosis inhibitor Necrostatin-1 (Fig. 6c and 6d). Triton X-100 fractionation assay revealed that knockdown of TRIM21 enhanced insoluble portion of p62 and Keap1 (Fig. 6e). The p62 binding-deficient W381/383A mutant and the E3 ligase-dead mutant C16A were stably transfected into H9c2 cells (Fig. 6f). While over-expression of WT TRIM21 led to decreased insoluble p62 and Keap1, the C16A or W381/383A did not (Fig. 6g). To further strengthen the human relevance of our findings, we determined the effect of TRIM21 on doxorubicin-induced cytotoxicity in an immortalized human cardiomyocyte line AC16 [48-50]. Consistent with our in vivo data (Fig. 3a), silence of TRIM21 led to increased NQO1 expression upon doxorubicin treatment (Suppl. Fig. S3a and S3b). Similar as in MEFs (Fig. 5a) and H9c2 (Fig. 6b), TRIM21-deficient AC16 cells were protected from doxorubicin-induced cell death (Suppl. Fig. S3c and S3d), which was inhibited by the ferroptosis inhibitor ferrostatin-1 and the iron chelator dexrazoxane but not the apoptosis inhibitor zVAD or necroptosis inhibitor Necrostatin-1 (Suppl. Fig. S3e). Together, these data indicate that TRIM21 negatively regulates p62-Keap1 aggregation and the anti-ferroptotic effect in cardiomyocytes.

Lastly, to test whether increased Nrf2 plays an important role in doxorubicine resistance in TRIM21-deficient cells, we treated TRIM21 WT and KO MEFs (Suppl. Fig. S4a) and TRIM21-deificient AC16 cells (Suppl. Fig. S4b) with the Nrf2 inhibitor ML385, or silenced Nrf2 with shRNA in MEFs (Suppl. Fig. S5a and S5b) and in AC16 cells (Suppl. Fig. S5c and S5d). Both pharmacological inhibition and genetic silencing of Nrf2 re-sensitized TRIM21-deficient MEFs and AC16 cells to doxorubicin treatment (Suppl. Fig. S4 and S5). These results further confirmed that doxorubicin-resistance conferred by TRIM21 deficiency is mediated by increased Nrf2 activity.

4. Discussion

Adverse cardiovascular events are recognized as the main cause of treatment-associated morbidity and mortality among cancer survivors. This is especially related to doxorubicin as a primary cardiotoxic chemotherapeutic agent [1,4,7,51]. Here we report that TRIM21 knockout mice are protected from doxorubicin-induced heart failure and animal fatality. Our previous study demonstrated that TRIM21 directly interacts with and ubiquitylates p62 at the lysine (K)7 residue to abolish its sequestration of Keap1 [28]. In the current study, our findings demonstrate that loss of TRIM21 enhances p62 sequestration function thus promotes p62-Keap1 aggregation, which stabilizes Nrf2 and increases the antioxidant capacity in the heart upon doxorubicin treatment. Interestingly, recent study shows that the Keap1-Nrf2 antioxidant response is disrupted upon doxorubicin exposure in vivo [14]. Nrf2 has been shown to play a protective role in oxidative stress-related cardiac diseases such as angiotensin II-induced cardiac hypertrophy, pressure overload, and ischemia/reperfusion injury [17,52,53]. Nrf2-deficient mice are more prone to doxorubicin-induced cardiotoxicity and cardiac dysfunction [54]. Moreover, both tumor susceptibility gene 101 (Tsg101) and Urolithin B (one of the gut metabolites of ellagitannins) protects against myocardial ischemia-reperfusion (I/R) injury through p62-Keap1-Nrf2 pathway [55,56]. Several natural compounds such as a-linolenic acid and sulforaphane were reported to suppress doxorubicin-induced cardiotoxicity through Keap1-Nrf2 pathway [57,58]. Consistent with these findings, our study demonstrates that the inhibition of TRIM21 can lead to activation of Nrf2 hence plays a protective role in doxorubicin-induced cardiotoxicity and suggests TRIM21 as a potential therapeutic target. This may be of particular interest in cancers where TRIM21 plays pro-tumorigenic roles. Along this direction, despite TRIM21's versatile biological functions, TRIM21 has been found to be pro-tumorigenic in various cancers by promoting proteasomal degradation of a tumor suppressor SGSMS1,[59] to protect cancer cell lines from cisplatin-induced cell death by interacting with Par-4,[60] to mediate degradation of the tumor suppressor CCAAT/enhancer-binding protein alpha (C/EBPα)[61], and to stabilize p53 through mediating non-degradative ubiquitination of guanosine 5'- monophosphate synthase (GMPS) [62]. Selectively inhibiting TRIM21 in these contexts may be beneficial by facilitating the chemotherapeutic anti-cancer effect and reducing the adverse cardiac toxicity.

Our results also indicate that targeting TRIM21 can protect cardiomyocytes from doxorubicin-induced ferroptosis. Despite the several mechanisms that have been described to account for doxorubicin cardiotoxicity including apoptosis, autophagy, and necroptosis, [23,25,26] recent studies demonstrate that ferroptosis inhibitor ferrostatin-1 can markedly reduce doxorubicin-induced mortality,

was used to compare the results. n.s., non-significant; ****p<0.0001. (g) Cells were lysed in IP lysis buffer containing 1% Triton X-100. The insoluble fraction was dissolved in RIPA buffer containing 1% SDS. Both the Triton X-100 soluble and insoluble fractions were subjected to WB. α-tubulin was probed as a marker of the soluble fraction. The WB bands were quantified by ImageJ, and the ratio of insoluble to soluble p62 and Keap1, respectively, is shown at the bottom.

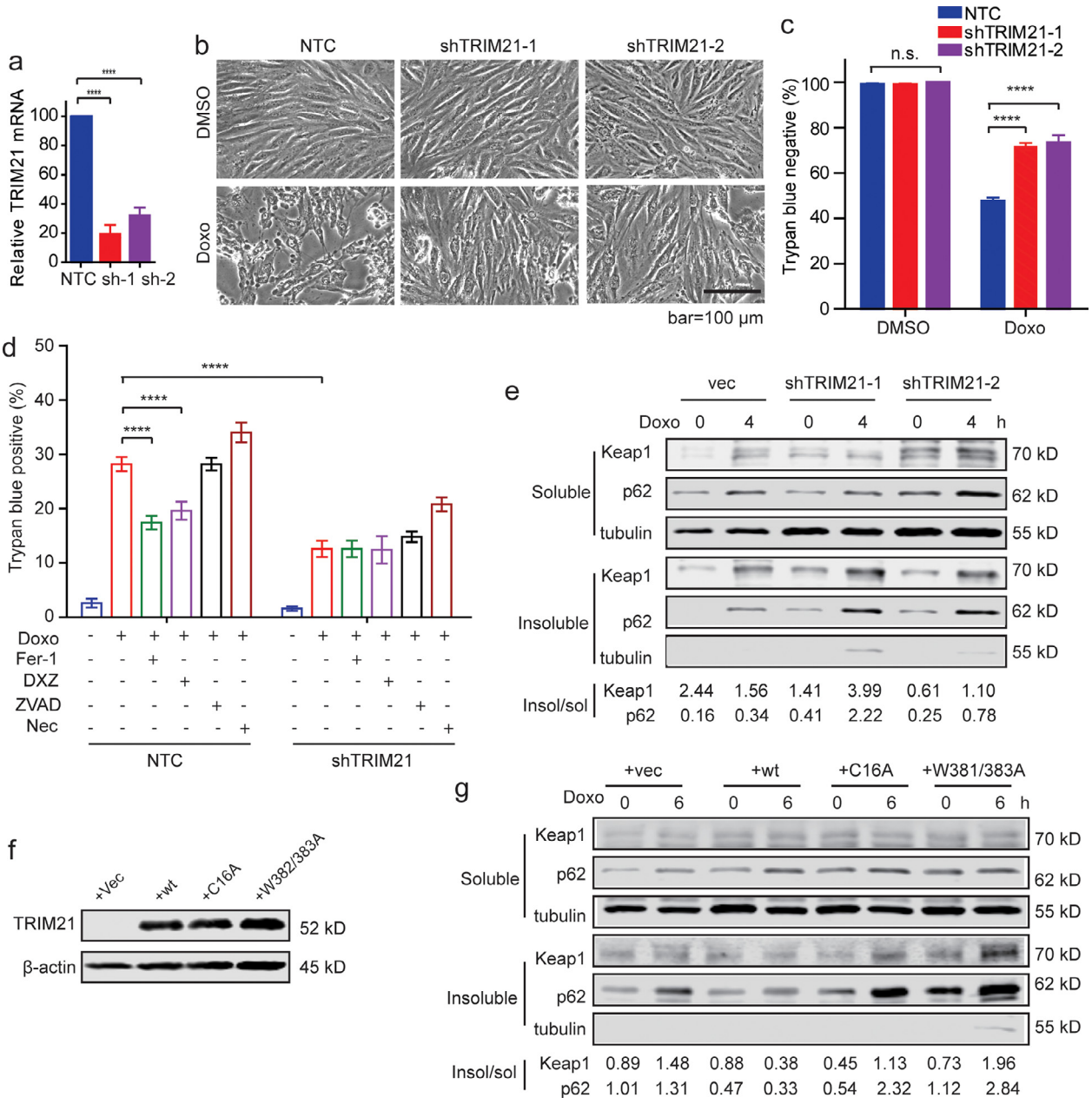

Fig. 6. TRIM21 negatively regulates p62-Keap1 aggregation and anti-ferroptotic effect in cardiomyocytes. (a) H9c2 immortalized rat cardiomyocytes were infected with lentiviral none-target control (shNTC) or two independent shRNAs for TRIM21. Relative mRNA level of TRIM21 was measured by quantitative RT-PCR. Data shown are mean ± standard deviation. Student's t-test was used to compare the results. ****$p<0.0001$. (b) Cells were treated with doxorubicin (1 μM) for 48 hours and observed under phase-contrast microscope. (c) Cell death was determined by trypan blue staining. Data shown are the mean plus SD of three countings (500 cells each). Student's t-test was used to compare the results. n.s., non-significant; ****$p<0.0001$. (d) H9c2 cells infected with lentiviral shNTC or shTRIM21 were treated with or without doxorubicin (Doxo, 1μM) alone or together with ferrostatin-1 (Fer-1,10 μM), DXZ (100 μM), zVAD (10 μM), or necrostatin-1 (Nec, 0.5 μM). Cell death was determined by trypan blue staining after 36 h. Shown is the average plus SD of triplicate experiments. Student's t-test was used to compare the results. n.s., non-significant; ****$p<0.0001$. (e) H9c2 cells infected with lentiviral shNTC or shTRIM21 were treated with doxorubicin (1 μM) for 4 h. Cells were lysed in IP lysis buffer containing 1% Triton X-100. The insoluble fraction was dissolved in RIPA buffer containing 1% SDS. Both the Triton X-100 soluble and insoluble fractions were subjected to IB. The ratio of insoluble to soluble bands was determined by ImageJ. (f) HA-TRIM21WT, HA-TRIM21C16A or HA-TRIM21W381/383A mutants was overexpressed in H9c2 cells. (g) H9c2 cells reconstituted with vector, HA-TRIM21WT, HA-TRIM21C16A or HA-TRIM21W381/383A mutants were treated with doxorubicin (1 μM) for indicated times. Cells were lysed in IP lysis buffer containing 1% Triton X-100. The insoluble fraction was dissolved in RIPA buffer containing 1% SDS. Both Triton X-100 soluble and insoluble fractions were subjected to IB. The ratio of insoluble to soluble bands was determined by ImageJ.

whereas no significant protection was observed in mice treated with emricasan (an inhibitor of apoptosis), necrostatin-1 (Nec-1, a specific inhibitor of receptor interacting protein kinase 1-mediated necroptosis), or 3-methyladenine (3-MA, an inhibitor of autophagy) [24]. Ferroptosis is initiated by severe lipid peroxidation, which relies on ROS generation and iron availability and is critically controlled by integrated oxidation and antioxidant systems [63]. Ferroptotic cells often display necrosis-like changes, such as cell swelling, plasma membrane rupture, and mitochondrial injury, which are different from apoptotic cells that are characterized by membrane blebbing and shrinkage [27,63]. Biochemically, ferroptosis is characterized by elevated levels of iron-dependent lipid peroxidation, indicated by the level of 4-HNE and MDA [27,64,65]. In our study, upon doxorubicin treatment, hearts from wild-type mouse exhibit ferroptotic features including deformed mitochondrial cristae, compromised membrane integrity, and elevated level of MDA and 4-HNE, which are alleviated in TRIM21 knockout mouse. These observations are consistent with the essential role of ferroptosis in doxorubicin-induced

cardiotoxicity, and are consistent with the protective role of the p62-Keap1-Nrf2 antioxidant pathway in ferroptosis in response to various ferroptotic inducers [66,67]

It needs to be cautioned that TRIM21, as a ubiquitin E3 ligase that promotes proteasomal degradation of numerous proteins, may exert the anti-ferroptotic function by regulating other pathways. One such possibility is through its regulation of immune system. TRIM21 was initially discovered as an antigen of autoantibody to the ribonucleoprotein Ro/SSA [68]. It has been implicated in autoimmune diseases such as systemic lupus erythematosus (SLE) and Sjogren syndrome [68,69]. TRIM21 can interact with numerous proteins involved in both innate and adaptive immunity. It was recently shown that TRIM21 deficiency in hematopoietic cell lineage leads to stable phenotype of atherosclerotic plaques through increased T cell-mediated IL-17 responses in the mouse model of atherosclerosis [70]. While doxorubicin-mediated cardiotoxicity is mainly explained by the cytotoxic effect on myocardium, inflammation of myocardium may also play an important role [1]. High mobility group box 1 (HMGB1), a damage-associated molecular pattern (DAMP), was reported to be released by stressed cells and drives inflammation by activating macrophages to produce pro-inflammatory cytokines [63,71]. Therefore, in addition to the protective role of TRIM21 ablation on oxidative damage/death via activation of the p62-Keap1-Nrf2 pathway, TRIM21's impact on proinflammatory response in this regard also needs investigation. Generation of TRIM21/Nrf2 double knockout mice may help clarify these possibilities.

Research in context

Evidence before this study: Cardiotoxicity is a major adverse effect in doxorubicin-based chemotherapy, which is thought to be caused by various forms of cell death resulting from oxidative stress. Previous studies show that the p62-Keap1-Nrf2 pathway plays a critical role in maintaining intracellular redox balance, and that the ubiquitin E3 ligase TRIM21 negatively regulates this antioxidant pathway. TRIM21 has been found to play important roles in immune response and in cancers, it is unknown whether TRIM21 has an effect on doxorubicin-induced cardiotoxicity, and if it does, what is the underlying mechanism.

Added value of this study: Using TRIM21 gene knockout mice, we found that TRIM21 ablation has a strong protective effect in oxidative cardiotoxicity induced by doxorubicin and LAD ligation. We further found that the cardiac protective effect upon doxorubicin treatment is through the inhibition of ferroptosis both *in vivo* and in cultured cells. As TRIM21 ubiquitylates p62 and negatively regulates the Keap1-Nrf2 antioxidant pathway, TRIM21-deficient mice and cells display increased antioxidant capacity, which can be reverted by the reconstitution of wild-type TRIM21 but not the ligase-dead and p62 interaction-deficient mutants.

Implications of all the available evidence: TRIM21 plays complex roles in immune response and cancer biology. In certain cancers, TRIM21 has been shown to be pro-tumorigenic. Our study demonstrates that TRIM21 ablation leads to cardiac protection from oxidative damages including that induced by the chemotherapeutic agent doxorubicin. Therefore, targeting TRIM21 be beneficial by reducing the adverse cardiac toxicity.

Contributors

KH performed most of the experiments and wrote the manuscript. JS, CZ, JZ, YZ, YJ performed experiments. JAP contributed methodology and experimental resources. YW performed data analysis. RZL, HC, and SG helped design experiments and provided technical assistance. SG performed data analysis and wrote the manuscript. WXZ conceptualized the general approach and wrote the manuscript. SG, HC, and WXZ have verified the underlying data. All authors have read and approved the final version of the manuscript.

Data sharing statement

The data that support the findings of this study are available from the corresponding author, Wei-Xing Zong, upon request.

Declaration of Competing Interest

The authors declare no competing interests.

Acknowledgements

We thank Dr. Keiko Ozato (NIH) for the TRIM21 KO mouse strain [38]. We also thank the innovative research team of high-level local university in Shanghai for their insightful support. The study was supported by NIH (CA129536; DK108989), Shanghai Pujiang Program (19PJ1401900), National Natural Science Foundation (31971161), Department of Veteran Affairs (BX004083) and Tianjin Science and Technology Plan Project (17ZXMFSY00020).

Supplementary materials

Supplementary material associated with this article can be found, in the online version, at doi:10.1016/j.ebiom.2021.103456.

References

[1] Herrmann J. Adverse cardiac effects of cancer therapies: cardiotoxicity and arrhythmia. Nat Rev Cardiol 2020;17(8):474–502.
[2] Tacar O, Sriamornsak P, Dass CR. Doxorubicin: an update on anticancer molecular action, toxicity and novel drug delivery systems. J Pharm Pharmacol 2013;65(2):157–70.
[3] Carvalho FS, Burgeiro A, Garcia R, Moreno AJ, Carvalho RA, Oliveira PJ. Doxorubicin-induced cardiotoxicity: from bioenergetic failure and cell death to cardiomyopathy. Med Res Rev 2014;34(1):106–35.
[4] Henriksen PA. Anthracycline cardiotoxicity: an update on mechanisms, monitoring and prevention. Heart 2018;104(12):971–7.
[5] Swain SM, Whaley FS, Ewer MS. Congestive heart failure in patients treated with doxorubicin: a retrospective analysis of three trials. Cancer 2003;97(11):2869–79.
[6] Bristow MR, Thompson PD, Martin RP, Mason JW, Billingham ME, Harrison DC. Early anthracycline cardiotoxicity. Am J Med 1978;65(5):823–32.
[7] Zamorano JL, Lancellotti P, Rodriguez Munoz D, Aboyans V, Asteggiano R, Galderisi M, et al. 2016 ESC Position Paper on cancer treatments and cardiovascular toxicity developed under the auspices of the ESC Committee for Practice Guidelines: The Task Force for cancer treatments and cardiovascular toxicity of the European Society of Cardiology (ESC). Eur Heart J 2016;37(36):2768–801.
[8] Ma J, Wang Y, Zheng D, Wei M, Xu H, Peng T. Rac1 signalling mediates doxorubicin-induced cardiotoxicity through both reactive oxygen species-dependent and -independent pathways. Cardiovasc Res 2013;97(1):77–87.
[9] Berthiaume JM, Wallace KB. Adriamycin-induced oxidative mitochondrial cardiotoxicity. Cell Biol Toxicol 2007;23(1):15–25.
[10] Deavall DG, Martin EA, Horner JM, Roberts R. Drug-induced oxidative stress and toxicity. J Toxicol 2012;2012:645460.
[11] Tatlidede E, Sehirli O, Velioglu-Ogunc A, Cetinel S, Yegen BC, Yarat A, et al. Resveratrol treatment protects against doxorubicin-induced cardiotoxicity by alleviating oxidative damage. Free Radic Res 2009;43(3):195–205.
[12] Varricchi G, Ameri P, Cadeddu C, Ghigo A, Madonna R, Marone G, et al. Antineoplastic drug-induced cardiotoxicity: a redox perspective. Front Physiol 2018;9:167.
[13] Nordgren KK, Wallace KB. Keap1 redox-dependent regulation of doxorubicin-induced oxidative stress response in cardiac myoblasts. Toxicol Appl Pharmacol 2014;274(1):107–16.
[14] Nordgren KKS, Wallace KB. Disruption of the Keap1/Nrf2-antioxidant response system after chronic doxorubicin exposure in vivo. Cardiovasc Toxicol 2020;20(6):557–70.
[15] Moi P, Chan K, Asunis I, Cao A, Kan YW. Isolation of NF-E2-related factor 2 (Nrf2), a NF-E2-like basic leucine zipper transcriptional activator that binds to the tandem NF-E2/AP1 repeat of the beta-globin locus control region. Proc Natl Acad Sci U S A 1994;91(21):9926–30.
[16] Minelli A, Bellezza I, Conte C, Culig Z. Oxidative stress-related aging: a role for prostate cancer? Biochim Biophys Acta 2009;1795(2):83–91.
[17] Bellezza I, Giambanco I, Minelli A, Donato R. Nrf2-Keap1 signaling in oxidative and reductive stress. Biochim Biophys Acta Mol Cell Res 2018;1865(5):721–33.

[18] Itoh K, Wakabayashi N, Katoh Y, Ishii T, O'Connor T, Yamamoto M. Keap1 regulates both cytoplasmic-nuclear shuttling and degradation of Nrf2 in response to electrophiles. Genes Cells 2003;8(4):379–91.
[19] Komatsu M, Kurokawa H, Waguri S, Taguchi K, Kobayashi A, Ichimura Y, et al. The selective autophagy substrate p62 activates the stress responsive transcription factor Nrf2 through inactivation of Keap1. Nat Cell Biol 2010;12(3):213–23.
[20] Lau A, Wang XJ, Zhao F, Villeneuve NF, Wu T, Jiang T, et al. A noncanonical mechanism of Nrf2 activation by autophagy deficiency: direct interaction between Keap1 and p62. Mol Cell Biol 2010;30(13):3275–85.
[21] Russo M, Guida F, Paparo L, Trinchese G, Aitoro R, Avagliano C, et al. The novel butyrate derivative phenylalanine-butyramide protects from doxorubicin-induced cardiotoxicity. Eur J Heart Fail 2019;21(4):519–28.
[22] Zeng C, Duan F, Hu J, Luo B, Huang B, Lou X, et al. NLRP3 inflammasome-mediated pyroptosis contributes to the pathogenesis of non-ischemic dilated cardiomyopathy. Redox Biol 2020;34:101523.
[23] Zhang T, Zhang Y, Cui M, Jin L, Wang Y, Lv F, et al. CaMKII is a RIP3 substrate mediating ischemia- and oxidative stress-induced myocardial necroptosis. Nat Med 2016;22(2):175–82.
[24] Fang X, Wang H, Han D, Xie E, Yang X, Wei J, et al. Ferroptosis as a target for protection against cardiomyopathy. Proc Natl Acad Sci U S A 2019;116(7):2672–80.
[25] Lu L, Wu W, Yan J, Li X, Yu H, Yu X. Adriamycin-induced autophagic cardiomyocyte death plays a pathogenic role in a rat model of heart failure. Int J Cardiol 2009;134(1):82–90.
[26] Zhu W, Soonpaa MH, Chen H, Shen W, Payne RM, Liechty EA, et al. Acute doxorubicin cardiotoxicity is associated with p53-induced inhibition of the mammalian target of rapamycin pathway. Circulation 2009;119(1):99–106.
[27] Galluzzi L, Vitale I, Aaronson SA, Abrams JM, Adam D, Agostinis P, et al. Molecular mechanisms of cell death: recommendations of the Nomenclature Committee on Cell Death 2018. Cell Death Differ 2018;25(3):486–541.
[28] Pan JA, Sun Y, Jiang YP, Bott AJ, Jaber N, Dou Z, et al. TRIM21 Ubiquitylates SQSTM1/p62 and suppresses protein sequestration to regulate redox homeostasis. Mol Cell 2016;61(5):720–33.
[29] Langmead B, Salzberg SL. Fast gapped-read alignment with Bowtie 2. Nat Methods 2012;9(4):357–9.
[30] Liao Y, Smyth GK, Shi W. featureCounts: an efficient general purpose program for assigning sequence reads to genomic features. Bioinformatics 2014;30(7):923–30.
[31] Anders S, Huber W. Differential expression analysis for sequence count data. Genome Biol 2010;11(10):R106.
[32] Zhou Y, Zhou B, Pache L, Chang M, Khodabakhshi AH, Tanaseichuk O, et al. Metascape provides a biologist-oriented resource for the analysis of systems-level datasets. Nat Commun 2019;10(1):1523.
[33] Favreau-Lessard AJ, Blaszyk H, Jones MA, Sawyer DB, Pinz IM. Systemic and cardiac susceptibility of immune compromised mice to doxorubicin. Cardiooncology 2019;5:2.
[34] Ma ZG, Kong CY, Wu HM, Song P, Zhang X, Yuan YP, et al. Toll-like receptor 5 deficiency diminishes doxorubicin-induced acute cardiotoxicity in mice. Theranostics 2020;10(24):11013–25.
[35] Liu D, Ma Z, Di S, Yang Y, Yang J, Xu L, et al. AMPK/PGC1alpha activation by melatonin attenuates acute doxorubicin cardiotoxicity via alleviating mitochondrial oxidative damage and apoptosis. Free Radic Biol Med 2018;129:59–72.
[36] Zheng D, Su Z, Zhang Y, Ni R, Fan GC, Robbins J, et al. Calpain-2 promotes MKP-1 expression protecting cardiomyocytes in both in vitro and in vivo mouse models of doxorubicin-induced cardiotoxicity. Arch Toxicol 2019;93(4):1051–65.
[37] Hullin R, Metrich M, Sarre A, Basquin D, Maillard M, Regamey J, et al. Diverging effects of enalapril or eplerenone in primary prevention against doxorubicin-induced cardiotoxicity. Cardiovasc Res 2018;114(2):272–81.
[38] Yoshimi R, Chang TH, Wang H, Atsumi T, Morse 3rd HC, Ozato K. Gene disruption study reveals a nonredundant role for TRIM21/Ro52 in NF-kappaB-dependent cytokine expression in fibroblasts. J Immunol 2009;182(12):7527–38.
[39] Calvo E, Moreno V, Flynn M, Holgado E, Olmedo ME, Lopez Criado MP, et al. Antitumor activity of lurbinectedin (PM01183) and doxorubicin in relapsed small-cell lung cancer: results from a phase I study. Ann Oncol 2017;28(10):2559–66.
[40] Selleri S, Seltmann H, Gariboldi S, Shirai YF, Balsari A, Zouboulis CC, et al. Doxorubicin-induced alopecia is associated with sebaceous gland degeneration. J Invest Dermatol 2006;126(4):711–20.
[41] Gelderblom H, Blay JY, Seddon BM, Leahy M, Ray-Coquard I, Sleijfer S, et al. Brostallicin versus doxorubicin as first-line chemotherapy in patients with advanced or metastatic soft tissue sarcoma: an European Organisation for Research and Treatment of Cancer Soft Tissue and Bone Sarcoma Group randomised phase II and pharmacogenetic study. Eur J Cancer 2014;50(2):388–96.
[42] Schultheiss HP, Fairweather D, Caforio ALP, Escher F, Hershberger RE, Lipshultz SE, et al. Dilated cardiomyopathy. Nat Rev Dis Primers 2019;5(1):32.
[43] Tang WHW, Li DY, Hazen SL. Dietary metabolism, the gut microbiome, and heart failure. Nat Rev Cardiol 2019;16(3):137–54.
[44] Xue M, Joo YA, Li S, Niu C, Chen G, Yi X, et al. Metallothionein protects the heart against myocardial infarction via the mtorc2/FoxO3a/Bim pathway. Antioxid Redox Signal 2019;31(5):403–19.
[45] Badgley MA, Kremer DM, Maurer HC, DelGiorno KE, Lee HJ, Purohit V, et al. Cysteine depletion induces pancreatic tumor ferroptosis in mice. Science 2020;368(6486):85–9.
[46] Arora P, Wu C, Hamid T, Arora G, Agha O, Allen K, et al. Acute metabolic influences on the natriuretic peptide system in humans. J Am Coll Cardiol 2016;67(7):804–12.
[47] Sun Y, Yi W, Yuan Y, Lau WB, Yi D, Wang X, et al. C1q/tumor necrosis factor-related protein-9, a novel adipocyte-derived cytokine, attenuates adverse remodeling in the ischemic mouse heart via protein kinase A activation. Circulation 2013;128(11 Suppl 1):S113–20.
[48] Davidson MM, Nesti C, Palenzuela L, Walker WF, Hernandez E, Protas L, et al. Novel cell lines derived from adult human ventricular cardiomyocytes. J Mol Cell Cardiol 2005;39(1):133–47.
[49] Duft K, Schanz M, Pham H, Abdelwahab A, Schriever C, Kararigas G, et al. 17beta-Estradiol-induced interaction of estrogen receptor alpha and human atrial essential myosin light chain modulates cardiac contractile function. Basic Res Cardiol 2017;112(1):1.
[50] Zhang X, Ji R, Liao X, Castillero E, Kennel PJ, Brunjes DL, et al. MicroRNA-195 regulates metabolism in failing myocardium via alterations in sirtuin 3 expression and mitochondrial protein acetylation. Circulation 2018;137(19):2052–67.
[51] Saleh Y, Abdelkarim O, Herzallah K, Abela GS. Anthracycline-induced cardiotoxicity: mechanisms of action, incidence, risk factors, prevention, and treatment. Heart Fail Rev 2020.
[52] Li J, Zhang C, Xing Y, Janicki JS, Yamamoto M, Wang XL, et al. Up-regulation of p27 (kip1) contributes to Nrf2-mediated protection against angiotensin II-induced cardiac hypertrophy. Cardiovasc Res 2011;90(2):315–24.
[53] Smyrnias I, Zhang X, Zhang M, Murray TV, Brandes RP, Schroder K, et al. Nicotinamide adenine dinucleotide phosphate oxidase-4-dependent upregulation of nuclear factor erythroid-derived 2-like 2 protects the heart during chronic pressure overload. Hypertension 2015;65(3):547–53.
[54] Li S, Wang W, Niu T, Wang H, Li B, Shao L, et al. Nrf2 deficiency exaggerates doxorubicin-induced cardiotoxicity and cardiac dysfunction. Oxid Med Cell Longev 2014;2014:748524.
[55] Deng S, Essandoh K, Wang X, Li Y, Huang W, Chen J, et al. Tsg101 positively regulates P62-Keap1-Nrf2 pathway to protect hearts against oxidative damage. Redox Biol 2020;32:101453.
[56] Zheng D, Liu Z, Zhou Y, Hou N, Yan W, Qin Y, et al. Urolithin B, a gut microbiota metabolite, protects against myocardial ischemia/reperfusion injury via p62/Keap1/Nrf2 signaling pathway. Pharmacol Res 2020;153:104655.
[57] Yu X, Cui L, Zhang Z, Zhao Q, Li S. alpha-Linolenic acid attenuates doxorubicin-induced cardiotoxicity in rats through suppression of oxidative stress and apoptosis. Acta Biochim Biophys Sin (Shanghai) 2013;45(10):817–26.
[58] Bose C, Awasthi S, Sharma R, Benes H, Hauer-Jensen M, Boerma M, et al. Sulforaphane potentiates anticancer effects of doxorubicin and attenuates its cardiotoxicity in a breast cancer model. PLoS One 2018;13(3):e0193918.
[59] Zhang J, Li YQ, Guo R, Wang YQ, Zhang PP, Tang XR, et al. Hypermethylation of SHISA3 promotes nasopharyngeal carcinoma metastasis by reducing SGSM1 stability. Cancer Res 2019;79(4):747–59.
[60] Nguyen JQ, Irby RB. TRIM21 is a novel regulator of Par-4 in colon and pancreatic cancer cells. Cancer Biol Ther 2017;18(1):16–25.
[61] Grandinetti KB, Stevens TA, Ha S, Salamone RJ, Walker JR, Zhang J, et al. Overexpression of TRIB2 in human lung cancers contributes to tumorigenesis through downregulation of C/EBPalpha. Oncogene 2011;30(30):3328–35.
[62] Reddy BA, van der Knaap JA, Bot AG, Mohd-Sarip A, Dekkers DH, Timmermans MA, et al. Nucleotide biosynthetic enzyme GMP synthase is a TRIM21-controlled relay of p53 stabilization. Mol Cell 2014;53(3):458–70.
[63] Chen X, Li J, Kang R, Klionsky DJ, Tang D. Ferroptosis: machinery and regulation. Autophagy 2020:1–28.
[64] Zou Y, Li H, Graham ET, Deik AA, Eaton JK, Wang W, et al. Cytochrome P450 oxidoreductase contributes to phospholipid peroxidation in ferroptosis. Nat Chem Biol 2020;16(3):302–9.
[65] Yamada N, Karasawa T, Kimura H, Watanabe S, Komada T, Kamata R, et al. Ferroptosis driven by radical oxidation of n-6 polyunsaturated fatty acids mediates acetaminophen-induced acute liver failure. Cell Death Dis 2020;11(2):144.
[66] Sun Y, He L, Wang T, Hua W, Qin H, Wang J, et al. Activation of p62-Keap1-Nrf2 pathway protects 6-hydroxydopamine-induced ferroptosis in dopaminergic cells. Mol Neurobiol 2020;57(11):4628–41.
[67] Sun X, Ou Z, Chen R, Niu X, Chen D, Kang R, et al. Activation of the p62-Keap1-NRF2 pathway protects against ferroptosis in hepatocellular carcinoma cells. Hepatology 2016;63(1):173–84.
[68] Ben-Chetrit E, Chan EK, Sullivan KF, Tan EM. A 52-kD protein is a novel component of the SS-A/Ro antigenic particle. J Exp Med 1988;167(5):1560–71.
[69] Ben-Chetrit E, Fox RI, Tan EM. Dissociation of immune responses to the SS-A (Ro) 52-kd and 60-kd polypeptides in systemic lupus erythematosus and Sjogren's syndrome. Arthritis Rheum 1990;33(3):349–55.
[70] Brauner S, Jiang X, Thorlacius GE, Lundberg AM, Ostberg T, Yan ZQ, et al. Augmented Th17 differentiation in Trim21 deficiency promotes a stable phenotype of atherosclerotic plaques with high collagen content. Cardiovasc Res 2018;114(1):158–67.
[71] Wen Q, Liu J, Kang R, Zhou B, Tang D. The release and activity of HMGB1 in ferroptosis. Biochem Biophys Res Commun 2019;510(2):278–83.